Core–Shell Nanoparticles

Deutsche Ausgabe: DOI: 10.1002/ange.201600625
Internationale Ausgabe: DOI: 10.1002/anie.201600625

L-Arginine-Triggered Self-Assembly of CeO_2 Nanosheaths on Palladium Nanoparticles in Water

Xiao Wang[+], Yibo Zhang[+], Shuyan Song, Xiangguang Yang, Zhuo Wang, Rongchao Jin,* and Hongjie Zhang**

Abstract: *Pd@CeO_2 core–shell nanostructures with a tunable Pd core size, shape, and nanostructure as well as a tunable CeO_2 sheath thickness were obtained by a biomolecule-assisted method. The synthetic process is simple and green, as it involves only the heating of a mixture of $Ce(NO_3)_3$, L-arginine, and preformed Pd seeds in water without additives. Importantly, the synthesis is free of thiol groups and halide ions, thus providing a possible solution to the problem of secondary pollution by Pd nanoparticles in the sheath-coating process. The Pd/CeO_2 nanostructures can be composited well with γ-Al_2O_3 to create a heterogeneous catalyst. In subsequent tests of catalytic NO reduction by CO, Pd@CeO_2/Al_2O_3 samples based on Pd cubes (6, 10, and 18 nm), Pd octahedra (6 nm), and Pd cuboctahedra (9 nm) as well as a simply loaded Pd cube (6 nm)–CeO_2/Al_2O_3 sample were used as catalysts to investigate the effects of the Pd core size and shape and the hybrid nanostructure on the catalytic performance.*

The use of biomolecules as capping agents to assist the formation of inorganic nanoparticles (NPs) has become a hot topic of research.[1–5] DNA and other nucleic acids are the most commonly used. Since they contain functional groups capable of binding metallic NPs, nucleic acids have great impact on crystal growth, such as the stabilization of ultrasmall noble metals (NMs),[1] the induction of morphology evolution,[2] and assistance in the formation of self-assembled supperlattices.[3] In principle, this control provides a means of constructing highly functional materials with designed optical, magnetic, electronic, and catalytic properties. However, the extremely high cost of DNA and nucleic acids have seriously limited the application of this approach. The existence of similar functional groups in amino acids inspired us to develop a new synthesis by using a low-cost amino acid to control the crystal-growth process.

Our research group has continuously focused on the potential of ceria (CeO_2) owing to its numerous oxygen vacancy defects and high oxygen-storage capacity.[6–10] Cerium is highly earth-abundant and can readily convert between the III and IV oxidation states.[11] These properties have made CeO_2 the key oxygen-storage component of the three-way catalyst used in automotive catalytic converters for the elimination of engine-exhaust pollutants.[12] The use of CeO_2 as an excellent support for NMs has emerged as an attractive alternative with the required high activity for low-temperature water–gas shift (WGS) reactions, oxygen sensors, oxygen-permeation membrane systems, and fuel cells.[13] Furthermore, among various hybrid NM/CeO_2 materials, the NM@CeO_2 core@shell nanostructure has gained attention for its significantly increased catalytic activity and stability.[14–18] After densely coating with a CeO_2 sheath, the noble-metal core can be protected physically to prevent mass transformation during both synthesis and long-term catalytic cycling, especially in a high-temperature environment. In the typical Pd@CeO_2 system, some important advances have been made. Gorte, Fornasiero, and co-workers have made a significant contribution towards the design and synthesis of Pd@CeO_2 core@shell nanostructures by the use of thiol-protected Pd NPs as cores, and the controlled hydrolysis of a cerium(IV) alkoxide self-assembled around the Pd NPs to form CeO_2.[19–22] Our research group also found that uniform Pd@CeO_2 core–shell nanospheres can be fabricated through an autoredox reaction between $Ce(OH)_3$ and Na_2PdCl_4 with the help of a large amount of KBr as the salting-out agent.[7] Furthermore, Zheng and co-workers showed that unique Pd@CeO_2 multicore–shell nanostructures can be produced by using oil-soluble Pd NPs as seeds in conjunction with a coating–assembling–etching process (SiO_2 is used as a hard template in during synthesis by this approach).[23] However, the use of thiol groups and halide ions during the CeO_2 coating process can cause secondary pollution, which is very harmful for catalytic performance. Precise control is required, and the use of expensive and toxic organic surfactants and solvents should be avoided. Furthermore, the size and shape of Pd cores can still not be controlled well. Generally, the catalytic performance of Pd NPs can be optimized by tuning their particle size and the properties of exposed faces. However, no investigation of the effects of the size and shape of the Pd NPs in the core@shell nanostructures has been reported until now, as challenges still exist in the aqueous synthesis of high-quality monodisperse Pd@CeO_2

[*] Dr. X. Wang,[+] Dr. Y. Zhang,[+] Dr. S. Song, Prof. X. Yang, Dr. Z. Wang, Prof. H. J. Zhang
State Key Laboratory of Rare Earth Resource Utilization
Changchun Institute of Applied Chemistry
Chinese Academy of Sciences
Changchun 130022, Jilin (China)
E-mail: songsy@ciac.ac.cn
hongjie@ciac.ac.cn
Prof. R. Jin
Department of Chemistry, Carnegie Mellon University
Pittsburgh, PA 15213 (USA)
E-mail: rongchao@andrew.cmu.edu
[+] These authors contributed equally.

Supporting information for this article, including details of the synthetic methods, XRD and XPS data of the as-obtained products, TEM images of blank experiments, and additional catalytic test results, can be found under http://dx.doi.org/10.1002/anie.201600625.

core–shell nanostructures with controllable Pd cores and clean surface states.

Herein, we describe the use of the biomolecule L-arginine (Arg) as a capping agent to induce the self-assembly of CeO_2 nanosheaths on a variety of Pd NPs as cores. The whole synthetic process is carried out by mixing $Ce(NO_3)_3$, L-arginine, and presynthesized Pd NPs as seeds without additives of any kind (Figure 1). The choice of L-arginine resulted from the following considerations: 1) L-arginine is rich in functional groups capable of binding both Pd and CeO_2 NPs; 2) the guanidine group exists at the end of L-arginine and provides the excellent solubility in water; more importantly, the guanidine group can generate a large number of OH^- ions under aqueous conditions.

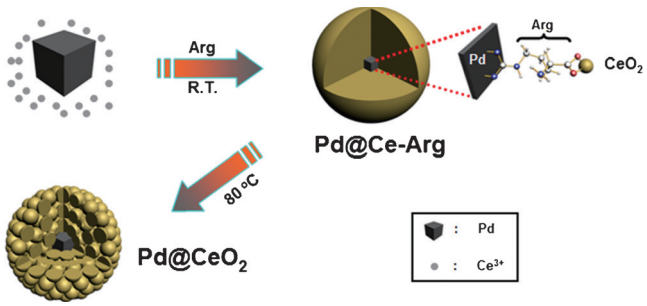

Figure 1. Synthesis of $Pd@CeO_2$ core–shell nanostructures.

As shown by a low-magnification TEM image (Figure 2A), uniform and monodisperse nanospheres with a narrow size distribution ((25 ± 3) nm) were formed by this method. No scattered CeO_2 NPs or uncoated Pd NPs were found. From Figure 2B, it is clear that these nanospheres have a typical core@shell superstructure. In each hybrid nanosphere, the shell is built up by numerous tiny CeO_2 NPs, which together form a complete sheath. The Pd cubes beneath the shell can be distinguished by their deeper contrast from CeO_2 (see Figure S1 in the Supporting Information for corresponding TEM images of 6 nm Pd cubes). Careful observation of the Pd cubes after the seeded growth process detected no obvious change in their size or shape. This result confirms that L-arginine is mild enough to maintain the original size and shape of the Pd cores.

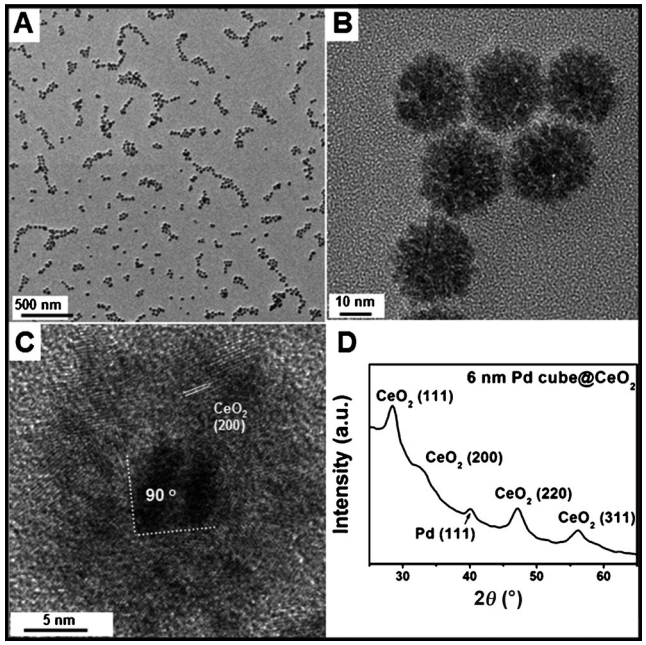

Figure 2. A,B) TEM images, C) HRTEM image, and D) XRD pattern of 6 nm $Pd@CeO_2$ core–shell nanostructures.

High-resolution TEM (HRTEM) showed that the lattice spacing of the shells (0.27 nm) corresponds well with the (200) planes of fluorite phase CeO_2 (Figure 2C). However, the dense CeO_2 coating makes it hard to observe any clear crystal planes of Pd in the core position; therefore, HAADF-STEM technology was used to further analyze the distribution of Pd and Ce components in the nanospheres. It was observed that the element Ce is spread everywhere and that Pd only exists in the center of the nanosphere (see Figure S2), thus confirming the synthesis of $Pd@CeO_2$ core–shell nanostructures. The peaks at $2\theta = 28.5$, 33.0, 47.4, and 56.3° in the XRD pattern of the 6 nm Pd cube@CeO_2 hybrid samples (Figure 2D) can be indexed to (111), (200), (220), and (311) CeO_2 fluorite-phase reflections (JCPDS No. 34-0394), respectively. The other strong peak at $2\theta = 40.1°$ corresponds to the pure (111) Pd reflections (JCPDS No. 46-1043). The two peaks at 881.9 and 900.2 eV observed by X-ray photoelectron spectroscopy (XPS; without any surface-etching treatment; see Figure S3) can be assigned as Ce $3d_{5/2}$ and $3d_{3/2}$ spin–orbit peaks, respectively. However, there was no clear peak observed between 350 and 330 eV (typical peaks of Pd), which is indirect evidence of core–shell nanostructures. Furthermore, the Pd content of the as-obtained $Pd@CeO_2$ core–shell nanospheres was 15.4 wt%, as determined by elemental analysis by inductively coupled plasma atomic emission spectrometry (ICP-AES). The specific surface area of the as-obtained $Pd@CeO_2$ sample, as calculated from the BET curve (see Figure S4), was approximately 74.2 $m^2 g^{-1}$. Such a large BET surface is possibly caused by the smaller size of whole hybrids with a porous sheath.

Interestingly, it was found that the hybrid structure is highly sensitive to the reaction temperature. A decrease in the reaction temperature from 80 to 60 °C can make the CeO_2 shell more branched (see Figure S5). To elucidate the growth mechanism, we also investigated the morphology evolution by following the addition of a solution of L-arginine at room temperature, without any heat treatment (Pd@Ce-Arg). In this case, no clear core@shell nanostructure was formed (see Figure S6A). Some parts have an approximate core–shell structure with Pd cubes in the core position, but a large number of tiny CeO_2 NPs are scattered everywhere. Furthermore, the corresponding XRD spectrum confirmed the formation of CeO_2 nanocrystals in the precursors (see Figure S6B). Thermogravimetric analysis (TGA) of Pd@Ce-Arg and 6 nm Pd cube@CeO_2 showed that 50 wt% of Pd@Ce-Arg was lost when the temperature increased to 800 °C (see Figure S6C); the weight loss of $Pd@CeO_2$ was approximately 7 wt%. The main inflection point in the two TGA spectra

appeared at the same temperature, approximately 250 °C (i.e. the decomposition temperature of L-arginine).

These results indicate that some amount of L-arginine molecules adsorbed on the surface of CeO_2 NPs, as well as free L-arginine molecules, play an important role in the formation of the original sheath. Subsequently, heat treatment is necessary to provide enough OH^- ions to slowly induce the complete hydrolysis of Ce^{3+} to build up a densely coated sheath. Therefore, the mechanism of formation of the Pd@CeO_2 core–shell nanostructures can be understood as follows: First, after the addition of L-arginine to the reaction solution, the guanidine group binds to the outer electronegative surface of the Pd cube, and the −COOH group at the other end of the bound L-arginine molecule can bind a Ce^{3+} ion. In this way, L-arginine molecules can readily bind large amounts of Ce^{3+} ions around the Pd cubes. When the amount of L-arginine molecules is increased, Ce^{3+} ions are hydrolyzed partially, and L-arginine functions as an adhesive to make CeO_2 assemble to form a sheath instead of participating in independent nucleation events. Then, when the reaction temperature is increased, L-arginine is able to provide enough OH^- ions to induce the hydrolysis of Ce^{3+} to form CeO_2 nanocrystals, and the as-formed CeO_2 nanocrystals assemble tightly with the loss of the L-arginine molecules. The final result is a densely coated and well-crystallized CeO_2 sheath with only minimal amounts of residual L-arginine molecules adsorbed on the surface of CeO_2 NPs.

We designed a series of control experiments to gain deeper insight into the generality of this L-arginine-assisted method. As shown in Figure 3 A–F, 10 nm and 18 nm Pd cubes were also successfully encapsulated by a CeO_2 shell. From Figure 3 C,F, it is clear that in the core position, the Pd cubes have sharp corners. According to a previous report,[24] Br^- ions could adsorb strongly onto the (100) surface of the Pd cube during synthesis. To study the influence of the adsorption, we used only polyvinylpyrrolidone-protected irregular Pd NPs without Br^- capping cubes as seeds in the seeded growth process. As shown in Figure 3 G–I, changing of the capping agent does not impede the formation of core–shell nanostructures. Uniform Pd NP@CeO_2 samples were also obtained. Furthermore, other kinds of Pd NPs could be embedded into CeO_2 nanospheres by this synthetic strategy. Thus, one-dimensional Pd nanowire@CeO_2 (Figure 3 J–N), 9 nm Pd cuboctahedron@CeO_2 (see Figure S7), and 6 nm Pd octahedron@CeO_2 (see Figure S8) core–shell nanostructures were successfully synthesized. Finally, the thickness of the CeO_2 shell could also be controlled well by directly changing the feeding amount of Ce (see Figure S9 for details).

Before catalytic testing, the as-obtained Pd@CeO_2 samples with different Pd core sizes were loaded on commercial γ-Al_2O_3 supports to further increase the catalytic performance of the Pd@CeO_2 nanospheres. The Pd@CeO_2 samples were loaded onto needlelike γ-Al_2O_3 uniformly, and they maintained the original monodispersity (see Figure S10 A for TEM images). No scattered or agglomerated NPs were found. The anti-sintering characteristics of the as-obtained 6 nm Pd@CeO_2/Al_2O_3 were first examined by calcination at 600 °C for 5 h in air. By comparing TEM images, it was found that there were no changes in size, shape, or the hybrid

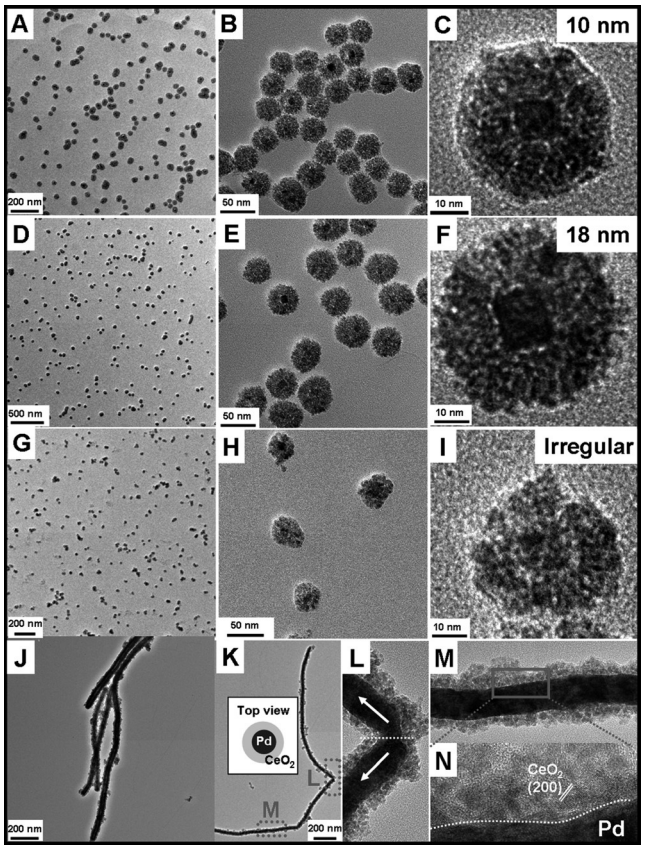

Figure 3. TEM images of A–C) 10 nm Pd cube@CeO_2, D–F) 18 nm Pd cube@CeO_2, G–I) irregular Pd@CeO_2, and J–N) Pd nanowires@CeO_2. Scale bars: A) 200, B) 50, C) 10, D) 500, E) 50, F) 10, G) 200, H) 50, I) 10, J) 200, K) 200 nm.

nanostructure (Figure S10 B). Moreover, no agglomeration occurred. The excellent anti-sintering ability of Pd@CeO_2 could be attributed to strong protection by the CeO_2 sheath, as well as the support effect of commercial Al_2O_3.

The catalytic reaction $CO + NO \rightarrow CO_2 + N_2$ has received increased attention because of its dual effect of reducing NO and oxidizing CO at the same time.[25] It is one of the first model reactions investigated in the field of three-way catalysts and dates back many decades.[26] However, the catalytic reduction of NO by CO is more challenging than the traditional model reaction of CO oxidation and requires a catalyst with higher activity, stability, and selectivity. Catalytic activity was evaluated by the use of a fixed-bed reactor coupled with mass spectrometry. Figure 4 shows the rate data for NO reduction over six kinds of Pd–CeO_2 hybrid samples, which had previously been loaded on commercial Al_2O_3: 6 nm Pd cube@CeO_2, 10 nm Pd cube@CeO_2, 18 nm Pd cube@CeO_2, 9 nm Pd cuboctahedron@CeO_2, 6 nm Pd octahedron@CeO_2, and 6 nm Pd–CeO_2 (simply loaded form). Rapid and almost linear evolution is observed between ln(rate) and $1/T$, thus indicating that the catalytic reaction is a typical first-order reaction. The kinetic data in Figure 4 can be divided into three different regions.

In region I, the reaction rate decreases with increasing size of the Pd core (see Figure S11 for the corresponding light-off

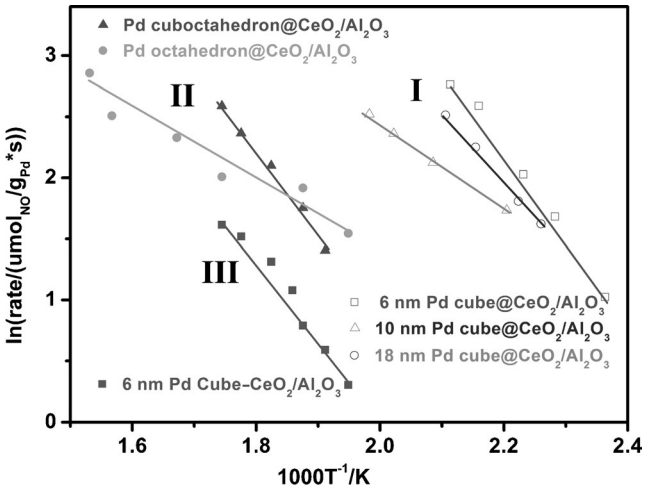

Figure 4. Kinetic data. Arrhenius-type plots for NO reduction by CO over 6 nm Pd cube@CeO_2/Al_2O_3, 10 nm Pd cube@CeO_2/Al_2O_3, 18 nm Pd cube@CeO_2/Al_2O_3, 9 nm Pd cuboctahedron@CeO_2/Al_2O_3, 6 nm Pd octahedron@CeO_2/Al_2O_3, and simply loaded 6 nm Pd cube–CeO_2/Al_2O_3. The rates of the catalysts are calculated on the basis of the total mass of the Pd metal. The Pd content in these nanocatalysts was determined by ICP analysis (see Table S1).

curves). It is typical size-dependent catalytic performance that the smaller a Pd core is, the greater is its catalytic activity. To intuitively display the size effect, metal dispersion data was obtained by CO pulse experiments at room temperature. The values found were 5.59, 4.93, and 3.40% for the 6, 10, and 18 nm Pd cube@CeO_2/Al_2O_3 sample, respectively. Thus, according to the metal dispersion data, the rates of these three kinds of nanocatalysts with different Pd core sizes were calculated to be 206×10^{-6}, 183×10^{-6}, and 164×10^{-6} mol$(g_{Pd,\ active\ sites}s)^{-1}$, respectively, at a reaction temperature of 192 °C.

In region II, the different catalytic performance could mainly be attributed to a shape effect. It is well-known that a Pd cube and a Pd octahedron are enclosed by six (100) and eight (111) faces, respectively. This catalytic result firmly confirmed that Pd (100) faces have much higher catalytic ability than Pd (111) faces. Since a Pd cuboctahedron has six (111) and six (100) faces, this kind of core–shell nanocatalyst exhibited medium catalytic performance. However, such size and shape effects are much weaker than the structure effect. As shown in region III, the simply loaded 6 nm Pd cube–CeO_2 catalyst showed the poorest catalytic performance.

To find an explanation for this structure effect, we undertook CO temperature-programmed desorption (CO-TPD) and quantitative H_2 temperature-programmed reduction (H_2-TPR) analysis. For the as-obtained 6 nm Pd cube@-CeO_2 sample, a strong peak was observed at 233.7 °C (see Figure S12), which is the expected temperature for CO desorption from Pd.[27] In contrast, for the simply loaded 6 nm Pd–CeO_2/Al_2O_3 hybrid nanomaterial, the intensity of the desorption peak was much weaker. This result demonstrates that the core–shell materials have higher CO-desorption capabilities. Generally, for Pd catalysts, CO species adsorb strongly on the Pd surface in the low-temperature region, and the reaction rate is controlled by the desorption of CO.[28] The faster the CO gas desorbs, the higher catalytic activity it has. The result of CO-TPD analysis suggests that the higher catalytic activity of the Pd@CeO_2 core–shell materials most likely results from their higher CO-desorption capability as compared to that of the simply loaded material. In the H_2-TPR profiles of the core–shell NPs (see Figure S13), a sharp peak corresponding to the reduction of PdO species on the CeO_2 surface appeared at 41.5 °C, and a negative peak corresponding to the decomposition of palladium hydride appeared at about 80.6 °C, whereas the simply loaded Pd–CeO_2 sample exhibited a similar H_2-consumption peak at about 52.7 °C. Another broad positive peak was also observed at about 94.1 °C. These different peak positions indicate variation in the distribution of PdO with support composition.[29] According to previous reports,[30,31] it is suggested that the H_2-TPR peak of the Pd–CeO_2/Al_2O_3 sample at 52.7 °C could be attributed to the reduction of PdO species on Ce–Al–O surfaces. H_2 consumption for these peaks was calculated by using CuO as a standard. A consumption of 0.25 mmol g^{-1} was measured for the core–shell sample (see Table S2), which is clearly lower than the 0.42 mmol g^{-1} expected theoretically for PdO production (Pd content: 4.5 wt% in Pd@CeO_2/Al_2O_3), thus indicating that the Pd exists partially in the form of Pd metal. On the other hand, the simply loaded sample shows a higher consumption of 0.72 mmol g^{-1} than the 0.45 mmol g^{-1} expected for theoretical PdO production (Pd content: 4.8 wt% in Pd@CeO_2/Al_2O_3), possibly as a result of the concurrent reduction of surface Ce^{4+}. This result confirmed that the formation of the Pd@CeO_2 core–shell nanostructure can increase the stability of Pd metal and the reducibility of PdO species. Thus, the core–shell materials exhibit remarkably enhanced catalytic performance relative to that of the simply loaded materials.

A nowadays widely accepted possible mechanism of such catalytic reactions involves Ce^{3+} in an important role: NO can reoxidize Ce^{3+} to Ce^{4+}, and CO can subsequently reduce Ce^{4+} to Ce^{3+}.[32,33] In an XPS spectrum of the 6 nm Pd cube@CeO_2/Al_2O_3 sample after the catalytic reaction, an Ce^{3+} signal was also clearly observed (see Figure S14), thus indicating that Ce^{3+} participates in the catalytic reaction. Previous studies have shown that N_2O is the main by-product. Thus, we collected the gas mixture during catalysis at different temperatures and analyzed the N_2O content by high-performance liquid chromatography after precolumn derivatization. For the 6 nm Pd cube@CeO_2 sample, the N_2O content was 5, 30, and 75 ppm at 100, 150, and 200 °C, respectively (see Table S3). The simply loaded Pd–CeO_2/Al_2O_3 material showed much poorer selectivity, thus indicating the importance of embedding the highly active Pd NPs in CeO_2 nanostructures not only for catalytic activity but also for selectivity.

In summary, high-quality Pd@CeO_2 core–shell nanospheres with tunable core size, shape, shell thickness, and hybrid nanostructure have been successfully fabricated in water by a low-cost and straightforward biomolecule-assisted method. Without the addition of any expensive and toxic specific ligands (especially thiols and halide ions), L-arginine plays the key role as a linker between CeO_2 and Pd. Moreover, L-arginine could also function as an adhesive to

make CeO_2 assemble to form the original sheath. The densely coated and well-crystallized CeO_2 sheath was formed by increasing the reaction temperature. Because of effective protection by the CeO_2 shell and the support effect of γ-Al_2O_3, the obtained Pd catalyst exhibited excellent high-temperature stability. In a model reaction of catalytic CO oxidation by NO, as-obtained 6 nm Pd cube@CeO_2/Al_2O_3 exhibited the best catalytic activity among the various kinds of Pd@CeO_2 core–shell nanostructures. The effects of the size and shape of the Pd core and the effects of the hybrid nanostructure on catalytic performance were studied in depth. We believe that our interesting findings can direct the design of novel functional core–shell nanocatalysts with high efficiency. Furthermore, such "biomolecule-assisted" strategies in the synthesis of inorganic NPs are expected to be of great significance in nanosynthesis for real-world applications.

Acknowledgements

We are grateful for financial aid from the National Natural Science Foundation of China (Grant Nos. 21301167, 21521092, 21401186, 51372242, 91122030, and 21210001), the National Key Basic Research Program of China (No. 2014CB643802), and Jilin Province Youth Foundation (20130522122JH).

Keywords: arginine · ceria · core–shell nanoparticles · heterogeneous catalysis · palladium

How to cite: *Angew. Chem. Int. Ed.* **2016**, *55*, 4542 – 4546
Angew. Chem. **2016**, *128*, 4618 – 4622

[1] L. Zhang, J. Zhu, S. Guo, T. Li, J. Li, E. Wang, *J. Am. Chem. Soc.* **2013**, *135*, 2403.
[2] J. Wu, L. Tan, K. Hwang, H. Xing, P. Wu, W. Li, Y. Lu, *J. Am. Chem. Soc.* **2014**, *136*, 15195.
[3] E. Auyeung, W. Morris, J. Mondloch, J. Hupp, O. Farha, C. Mirkin, *J. Am. Chem. Soc.* **2015**, *137*, 1658.
[4] L. M. Demers, M. Östblom, H. Zhang, N. H. Jang, B. Liedberg, C. A. Mirkin, *J. Am. Chem. Soc.* **2002**, *124*, 11248.
[5] A. P. Alivisatos, K. P. Johnsson, X. Peng, T. E. Wilson, C. J. Loweth, M. P. Bruchez, P. G. Schultz, *Nature* **1996**, *382*, 609 – 611.
[6] X. Wang, D. Liu, S. Song, H. Zhang, *J. Am. Chem. Soc.* **2013**, *135*, 15864.
[7] X. Wang, D. Liu, J. Li, J. Zhen, F. Wang, H. Zhang, *Chem. Sci.* **2015**, *6*, 2877.
[8] S. Song, X. Wang, H. Zhang, *NPG Asia Mater.* **2015**, *7*, e179.
[9] X. Wang, D. Liu, J. Li, J. Zhen, H. Zhang, *NPG Asia Mater.* **2015**, *7*, e158.
[10] X. Wang, X. Li, D. Liu, S. Song, H. Zhang, *Chem. Commun.* **2012**, *48*, 2885.
[11] C. Sun, H. Li, L. Chen, *Energy Environ. Sci.* **2012**, *5*, 8475.
[12] J. Kašpar, P. Fornasiero, M. Graziani, *Catal. Today* **1999**, *2*, 285.
[13] Q. Fu, H. Saltsburg, M. Flytzani-Stephanopoulo, *Science* **2003**, *301*, 935.
[14] J. Qi, J. Chen, G. D. Li, S. X. Li, Y. Gao, Z. Y. Tang, *Energy Environ. Sci.* **2012**, *5*, 8937.
[15] K. Yoon, Y. Yang, P. Lu, H. Peng, K. Masias, P. Fanson, C. Campbell, Y. Xia, *Angew. Chem. Int. Ed.* **2012**, *51*, 9543 – 9546; *Angew. Chem.* **2012**, *124*, 9681 – 9684.
[16] T. Kayama, K. Yamazaki, H. Shinjoh, *J. Am. Chem. Soc.* **2010**, *132*, 13154.
[17] S. Zhang, C. Chen, M. Cargnello, P. Fornasiero, R. Gorte, G. Graham, X. Pan, *Nat. Commun.* **2015**, *6*, 7778.
[18] M. Pagliaro, P. Fornasiero, *ChemCatChem* **2015**, *7*, 1979.
[19] M. Cargnello, J. Jaén, J. Garrido, K. Bakhmutsky, T. Montini, J. Gámez, R. Gorte, P. Fornasiero, *Science* **2012**, *337*, 713.
[20] N. Wieder, M. Cargnello, K. Bakhmutsky, T. Montini, P. Fornasiero, R. Gorte, *J. Phys. Chem. C* **2011**, *115*, 915.
[21] L. Adijanto, A. Sampath, A. Yu, M. Cargnello, P. Fornasiero, R. Gorte, J. Vohs, *ACS Catal.* **2013**, *3*, 1801.
[22] L. Adijanto, D. Bennett, C. Chen, A. Yu, M. Cargnello, P. Fornasiero, R. Gorte, J. Vohs, *Nano Lett.* **2013**, *13*, 2252.
[23] C. Chen, X. Fang, B. Wu, L. Huang, N. Zheng, *ChemCatChem* **2012**, *4*, 1.
[24] M. Jin, H. Liu, H. Zhang, Z. Xie, J. Liu, Y. Xia, *Nano Res.* **2011**, *4*, 83.
[25] S. Roy, M. Hegde, *Catal. Commun.* **2008**, *9*, 811.
[26] J. Kašpar, C. Leitenburg, P. Fornasiero, A. Trovarelli, M. Graziani, *J. Catal.* **1994**, *146*, 136.
[27] X. C. Guo, J. T. Yates, *J. Chem. Phys.* **1989**, *90*, 6761.
[28] H.-J. Freund, G. Meijer, M. Scheffler, R. Schlögl, M. Wolf, *Angew. Chem. Int. Ed.* **2011**, *50*, 10064 – 10094; *Angew. Chem.* **2011**, *123*, 10242 – 10275.
[29] B. Yue, R. Zhou, Y. Wang, X. Zheng, *Appl. Catal. A* **2005**, *295*, 31.
[30] M. Luo, X. Zheng, *Appl. Catal. A* **1999**, *189*, 15.
[31] M. Luo, Z. Hou, X. Yuan, X. Zheng, *Catal. Lett.* **1998**, *50*, 205.
[32] G. Ranga Rao, P. Fornasiero, R. Di Monte, J. Kašpar, G. Vlaic, G. Balducci, S. Meriani, G. Gubitosa, A. Cremona, M. Graziani, *J. Catal.* **1996**, *162*, 1.
[33] P. Fornasiero, G. Ranga Rao, J. Kašpar, F. L'Erario, M. Graziani, *J. Catal.* **1998**, *175*, 269.

Received: January 20, 2016
Published online: March 7, 2016

